Article:
Tuckett, Pete orcid.org/0000-0001-9953-2602, Sole, Andrew, Livingstone, Stephen et al. (3 more authors) (2025) Continent-wide mapping shows increasing sensitivity of East Antarctica to meltwater ponding. Nature Climate Change. 775–783. ISSN: 1758-678X

https://doi.org/10.1038/s41558-025-02363-5

nature climate change

Article

https://doi.org/10.1038/s41558-025-02363-5

Continent-wide mapping shows increasing sensitivity of East Antarctica to meltwater ponding

Received: 10 November 2022

Accepted: 27 May 2025

Published online: 4 July 2025

Check for updates

Peter A. Tuckett[1,2,3] ✉, Andrew J. Sole[1], Stephen J. Livingstone[1], Julie M. Jones[1], James M. Lea[4] & Ella Gilbert[5]

Surface meltwater is predicted to become increasingly important for Antarctic mass loss as atmospheric temperatures rise, due to its potential to influence ice dynamic, hydrofracture and radiative processes. However, our understanding of Antarctic surface meltwater is limited, with previous studies restricted in spatial or temporal scope. Here, using cloud computing, we produce an Antarctic-wide, monthly dataset of surface meltwater for 2006 to 2021. Surface meltwater covered 3,732 km^2 across Antarctica on average during each melt season, with 30% on grounded ice. High interannual variability in meltwater area across the Antarctic Peninsula and in East Antarctica correlates with large-scale modes of climate variability. In west Antarctica, meltwater area is comparatively low and this correlation is absent. An increase in the magnitude and variability of surface meltwater area without a coincident increase in modelled snowmelt in East Antarctica indicates that the ice-sheet surface might be becoming more favourable to meltwater ponding.

Surface meltwater will play a crucial role in the response of Antarctica to climate warming, because ponded water can promote ice-shelf breakup[1,2], enhance localized melting[3,4] and influence grounded ice dynamics[5–7]. Although first noted by Antarctic explorers in 1909[8], and subsequently identified at various locations using remote sensing[9,10], the recent revelation that surface water is widespread around the Antarctic margin[3,11] has spawned several studies of individual ice shelves[12–14], groups of ice catchments[15,16], and at ice-sheet spatial scales[11,17,18]. Antarctic-wide fluxes of meltwater production have been generated using satellites[19–21] and models[22,23]. However, a continent-wide surface meltwater area dataset with high temporal resolution and decadal time span is lacking, meaning that the multi-annual and seasonal evolution of surface hydrology at a continental scale remains poorly constrained[24]. We address this by providing a monthly, long-term (15-yr) assessment of surface meltwater across Antarctica, enabling a comprehensive assessment of trends and spatial patterns in meltwater area.

To capture seasonal and interannual variability, we mapped surface meltwater across the Antarctic continent in Google Earth Engine (GEE)[14] at monthly intervals. Every available Landsat 7 and 8 image was analysed between 2006 and 2021, totalling 133,497 images. To account for meltwater probably excluded as a result of variable image coverage and cloud cover, we used image visibility assessments (Methods) to scale up our mapped area results, generating 'estimated' surface meltwater area totals[14]. This approach produced a consistent time series of surface meltwater, spanning the entire continent. All meltwater areas stated in-text are 'estimated' rather than 'observed', as these are probably more representative of the true value. However, our scaling-up method has some inherent uncertainties and true meltwater area is probably somewhere between observed and estimated values (Supplementary Discussion 1). Our analysis produces the same conclusions regardless of which of these data are used (Supplementary Discussion 2).

[1]School of Geography and Planning, University of Sheffield, Sheffield, UK. [2]Department of Environment & Geography, University of York, York, UK. [3]School of Geography, University of Leeds, Leeds, UK. [4]Department of Geography and Planning, University of Liverpool, Liverpool, UK. [5]British Antarctic Survey, Cambridge, UK. ✉e-mail: pete.tuckett@york.ac.uk

https://doi.org/10.1038/s41558-025-02363-5

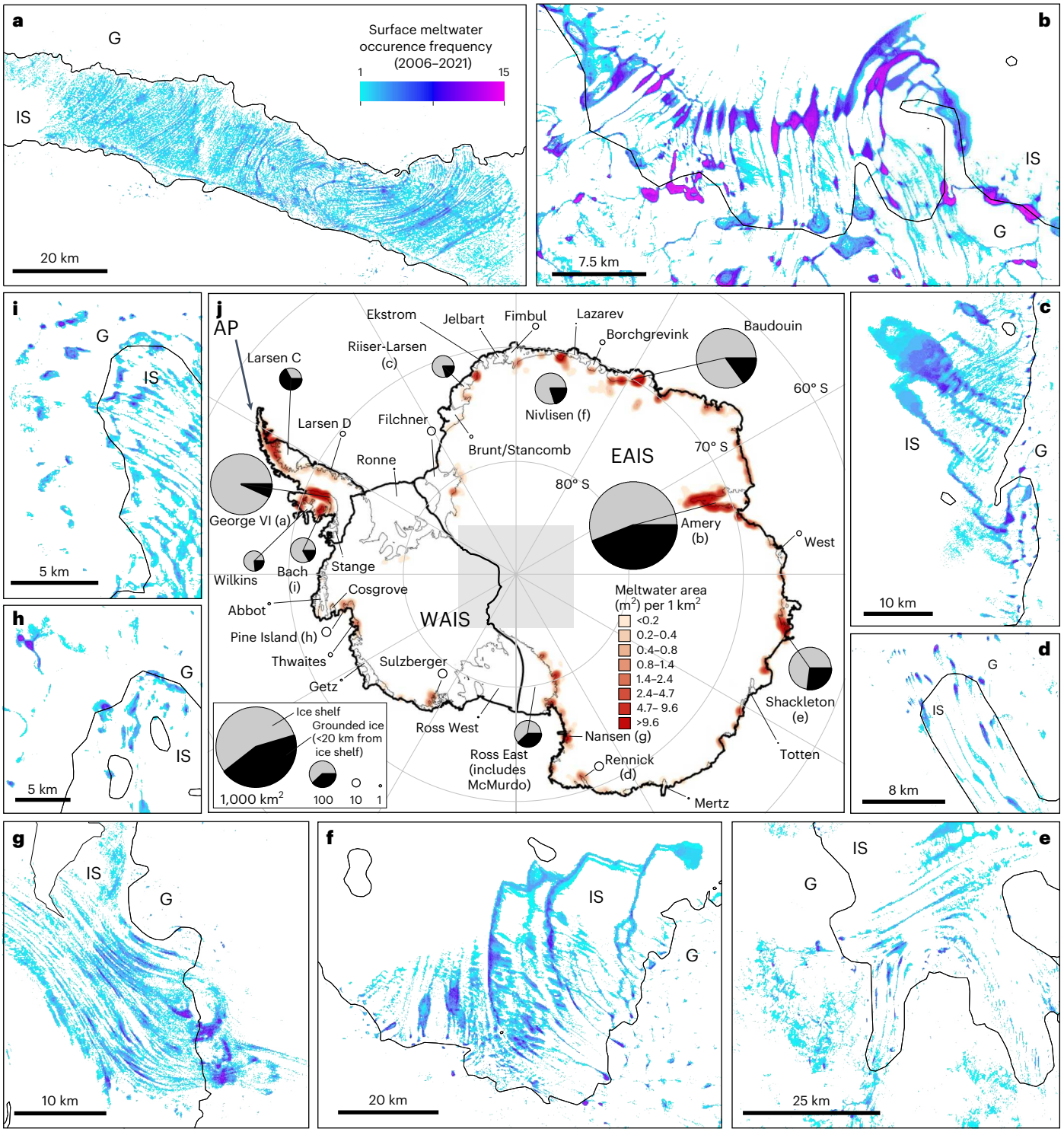

Fig. 1 | Surface meltwater around the Antarctic continent. a–i, Occurrence frequency of surface meltwater for key ice shelves (IS) and outlet glaciers (G): George VI Ice Shelf (**a**), Amery Ice Shelf (**b**), Riiser-Larsen Ice Shelf (**c**), Rennick Glacier (**d**), Shackleton Ice Shelf (**e**), Nivlisen Ice Shelf (**f**), Nansen Ice Shelf (**g**), Pine Island Ice Shelf (**h**) and Bach Ice Shelf (**i**). **j**, The location of each subpanel is shown in the central map: the spatial density of surface meltwater features across Antarctica, shown as mean meltwater area per 1-km^2 cell using a 50-km search radius. Circles associated with ice-shelf labels are sized proportionally to the average surface meltwater area of each named ice-shelf region, split between floating ice (grey) and grounded ice within 20 km of the grounding line (black). Pie charts are only displayed for ice-shelf regions with mean meltwater area >10 km^2. The thick black lines show the extent of the East and West Antarctic ice sheets and the AP. The central grey square indicates the region around the South Pole that was not mapped due to a lack of Landsat images (Methods). Ice-sheet and ice-shelf boundaries from ref. 56.

https://doi.org/10.1038/s41558-025-02363-5

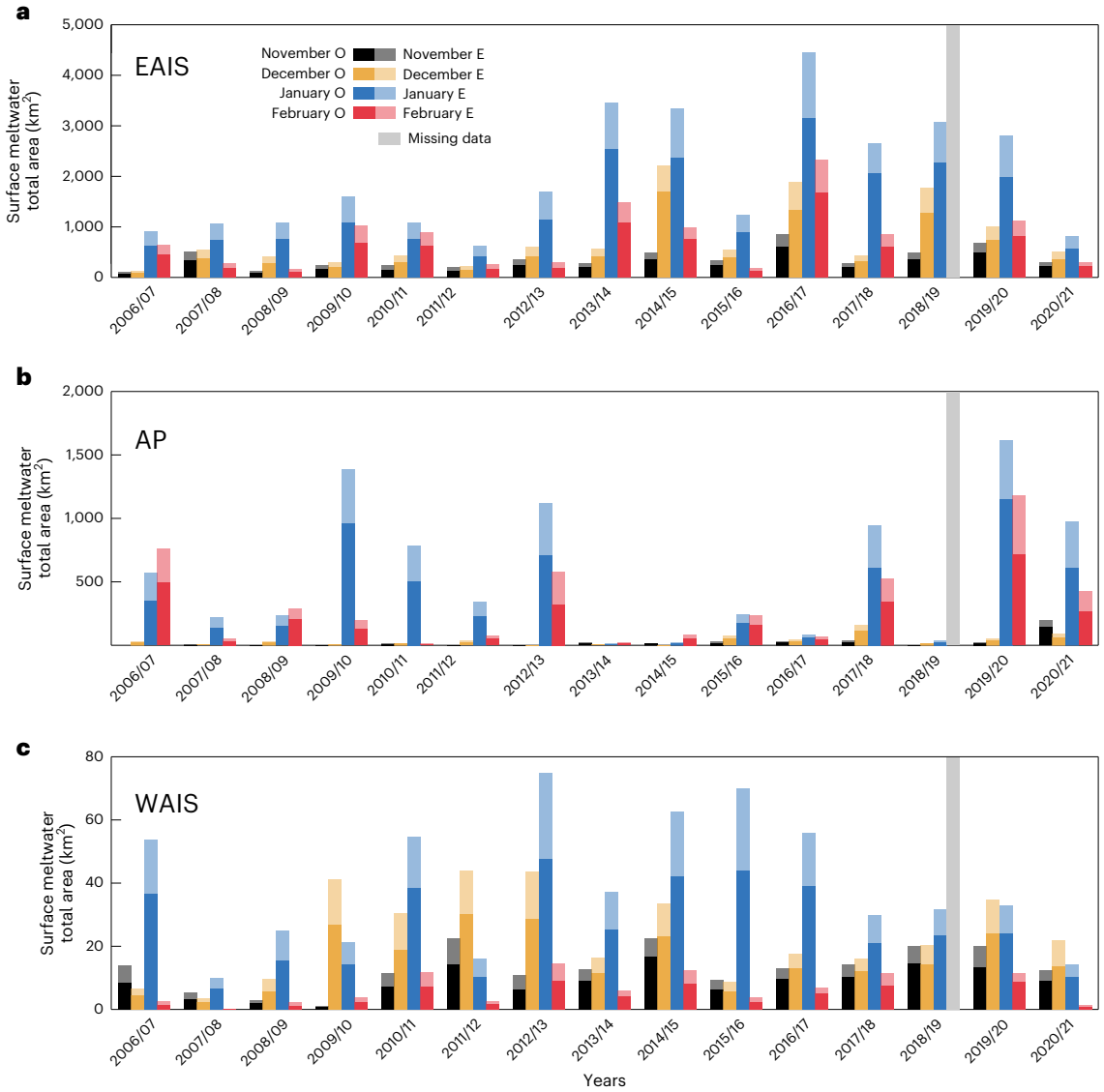

Fig. 2 | The seasonal and interannual evolution of surface meltwater across the Antarctic ice sheets from 2006 to 2021. a–**c**, EAIS (**a**), AP (**b**) and WAIS (**c**). Meltwater area data for November–February each melt season. Each opaque-coloured bar shows the observed (O) mapped surface meltwater area, with translucent bars displaying scaled up estimated (E) meltwater area based on visibility assessments (Methods).

Distribution of Antarctic meltwater

Ice-surface meltwater systems, comprising interconnected lakes, streams and regions of slush, occur around much of the Antarctic margin (Fig. 1). Surface water covered 3,732 km^2 (s.d. 1,547 km^2) of Antarctica on average (mean) each melt season, with 70% of water located on ice shelves. On the flatter topography of ice shelves, lakes are often elongate and connected by streams (Fig. 1a–i), with subtle along-flow topographic corrugations encouraging lakes to extend parallel with ice flow (Fig. 1e,g,i). Fewer, more isolated lakes occur in topographically confined basins on grounded ice and often reform in the same location in several years (Fig. 1b,i,g). The greatest surface meltwater area (annual maximum extent) was observed during the 2016/17 melt season, covering 4,574 and 2,218 km^2 of floating and grounded ice, respectively. By contrast, during the 2011/12 melt season, surface meltwater only covered 1,004 km^2 of floating ice and 516 km^2 of grounded ice.

The East Antarctic Ice Sheet (EAIS) has the largest area of surface meltwater (2,812 km^2 mean annual meltwater area; s.d. 1,478 km^2), representing ~0.03% of total EAIS area (grounded and floating area combined). EAIS-wide totals are dominated by large lakes (up to ~90 km^2) on ice shelves and their associated grounding zones, with 64% of total meltwater area situated on floating ice and 91% of water on grounded ice located within 20 km of the grounding line. Mean annual meltwater area totals are greatest for the Amery (1,110 km^2; s.d. 791 km^2), Roi Baudouin (516 km^2; s.d. 402 km^2), Shackleton (260 km^2; s.d. 192 km^2) and Nivlisen (138 km^2; s.d. 118 km^2) Ice Shelf regions, although with high variability between melt seasons (Extended Data Fig. 1). The proportion of each ice shelf covered in meltwater is nevertheless low; the highest being ~5% for Nivlisen Ice Shelf in 2007/08. The two largest EAIS ice shelves, Filchner and Ross (East), experience mean surface meltwater areas of 6 km^2 (s.d. 5 km^2) and 59 km^2 (s.d. 32 km^2), respectively.

The Antarctic Peninsula (AP) hosts the second highest meltwater area (855 km^2 mean; s.d. 665 km^2), although meltwater covers a greater proportion of the AP (~0.2%) than the EAIS (~0.03%). Complex meltwater networks often cover central sections of the George VI, Wilkins and Bach ice shelves (Fig. 1); the proportion of George VI Ice Shelf covered in meltwater each melt season (>2% median) is larger than any other ice shelf in Antarctica (Extended Data Fig. 1). While meltwater on the southern AP is concentrated on ice shelves, meltwater farther north on

https://doi.org/10.1038/s41558-025-02363-5

the AP is more abundant on grounded ice. For example, there is more meltwater on grounded ice surrounding the Larsen C Ice Shelf (<20 km inland of the grounding line), than on the ice shelf itself (Fig. 1j). Surface meltwater on grounded ice often includes extensive regions of slush (Extended Data Fig. 2g), which is abundant on the northeast outlet glaciers of the AP and glaciers feeding the southern AP ice shelves. Variability in the proportion of AP meltwater on grounded versus floating ice is far greater than either the West Antarctic Ice Sheet (WAIS) or EAIS, ranging from 1% on grounded ice in 2009/10 to 68% during the 2013/14 melt season (Extended Data Table 1).

Surface meltwater is less abundant on the WAIS, both in terms of absolute meltwater area (64 km^2 mean; s.d. 22 km^2) and proportionally (~0.002%). Peak surface meltwater area across the WAIS is typically 40–90 km^2 each melt season, with 2012/13 having the highest surface meltwater area total (105 km^2) of the study period (Fig. 2). Previously reported meltwater features around Pine Island, Cosgrove and Getz ice shelves[17] recur throughout our time series (Fig. 1g). Surface lakes of up to ~2 km^2 also commonly occur on grounded ice near nunataks surrounding Nickerson and Sulzberger ice shelves. On average, almost half (48% mean) of WAIS surface meltwater exists on grounded ice. No surface meltwater is detected around the eastern section of the Ross Ice Shelf or on any of the Siple Coast ice streams, despite the known occurrence of melt events within our study period[25].

Variability and trends in meltwater area

For the EAIS, WAIS and AP, meltwater area displays high interannual and seasonal variability. Around the EAIS, surface meltwater occurs throughout the austral summer (Fig. 2a) with a gradual increase in meltwater area throughout November and December, peaking in January, followed by a rapid decline during February (Fig. 2a). Annual variability in meltwater area is typically consistent between EAIS ice shelves, with notable exceptions[18]. For example, the greatest surface meltwater area for Nivlisen Ice Shelf occurred during the 2007/08 melt season when most of the EAIS experienced lower-than-average meltwater area (Fig. 3a). At the AP, there is typically negligible surface meltwater during November and December, before a rapid jump to a seasonal maximum in January. High meltwater area sometimes remains into February (Fig. 2b). The largest monthly meltwater area on the AP was in January 2020, consistent with record high meltwater area on George VI Ice Shelf[26]. Around the WAIS, surface meltwater area generally reaches a maximum in January, but peaked in December in 4 years when overall meltwater area was low (Fig. 2c).

For the EAIS, we observe an increase in both magnitude and variability of meltwater area across our 15-yr study period (Fig. 2a). Mean annual EAIS meltwater area between 2014 and 2021 (3,693 km^2; s.d. 1,493 km^2) was over double that of 2007–2013 (1,807 km^2; s.d. 534 km^2), despite 2015/16 and 2020/21 having low meltwater area (Fig. 2a). We find statistically significant increasing trends in EAIS meltwater area for our annual data (November–February maximum extent) and individually for the months of November and January (Extended Data Fig. 3). The greatest annual meltwater area occurred in 2016/17, when 5,945 km^2 of the EAIS was covered in meltwater at some stage during the melt season. There is no overall increase in meltwater area for either the AP or the WAIS, and these regions display contrasting patterns in meltwater area variability (Fig. 2). The WAIS is characterized by consistently low meltwater area, while the AP displays large variability between melt seasons; annual meltwater area ranged from 57 km^2 in 2013/14 to 2,330 km^2 in 2019/20.

Links with Antarctic climate

To investigate first-order atmospheric controls on continental-scale surface meltwater area, we compared our data to three modes of atmospheric variability known to influence Antarctic surface air temperatures: (1) the Southern Annular Mode (SAM); (2) the El Niño/Southern Oscillation (ENSO); and (3) the strength and location of the Amundsen Sea Low (ASL). The climate impacts of the three modes vary across Antarctica[27–29], so analysis was conducted separately for the EAIS, WAIS and AP. We also compared our data against modelled snowmelt from a statistically downscaled (2-km resolution) version[30] of the regional climate model RACMO2.3p2 (ref. 23). This enabled us to identify spatial and temporal differences in the proportion of snowmelt that gets translated into ponded meltwater.

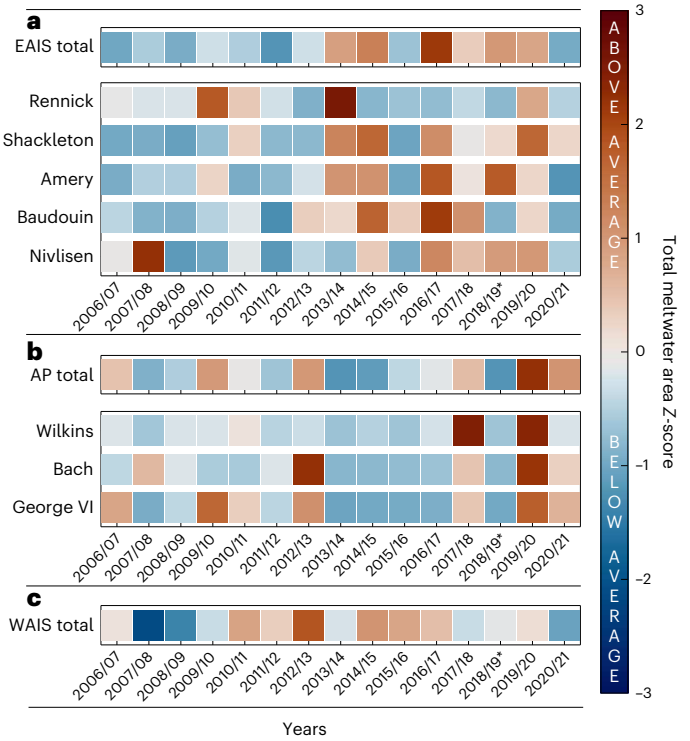

Fig. 3 | Interannual variability and trends in surface meltwater area from 2006 to 2021. a, *Z*-score anomalies relative to the 15-yr mean for the EAIS as a whole and for ice shelves with >0.5% meltwater coverage on average. **b**, *Z*-score anomalies as in **a** for the AP and individual ice shelves. **c**, *Z*-score anomalies as in **a** and **b** for the WAIS; note that no WAIS ice shelves have >0.5% meltwater coverage. *Z*-scores for 2018/19 are probably underestimated as a result of missing data in February 2019, highlighted by asterisks.

For the EAIS, we find a statistically significant negative correlation between the detrended summer SAM index and detrended maximum annual surface meltwater area ($r = -0.47$, $P = 0.02$), with greater meltwater area associated with negative SAM years (Fig. 4c). For the 6 years with the lowest SAM (<+0.7), median surface meltwater area was 20% greater than the 15-yr average (Fig. 4b). Conversely, the six lowest EAIS melt area years coincided with a strong positive summer SAM index (>+1.5) (Extended Data Table 2). EAIS surface meltwater area in the two most negative SAM years was 84% greater than the median (Extended Data Fig. 5d). The only year with a strong (<−1.5) negative SAM index (2016/17) corresponded with the highest annual meltwater area of the entire study period (Figs. 2a and 4a). No statistically significant correlations are found between EAIS surface meltwater area and ENSO or the ASL (Extended Data Fig. 4b–d).

At the AP, the strength and location of the ASL appears closely linked to the distribution and abundance of surface meltwater, as also shown for surface air temperatures and sea-ice extent[31]. Summer ASL relative central pressure (RCP) is negatively correlated ($r = -0.38$, $P < 0.001$) with surface meltwater area (Fig. 4c). Years with a deep ASL (<−8 RCP) result, on average, in surface meltwater area anomalies 102% greater than the median (Fig. 4d), while a weaker (>−6.5) ASL results in lower-than-average meltwater ponding on the AP (Extended Data Fig. 6a). Surface meltwater area is also typically greater when the

https://doi.org/10.1038/s41558-025-02363-5

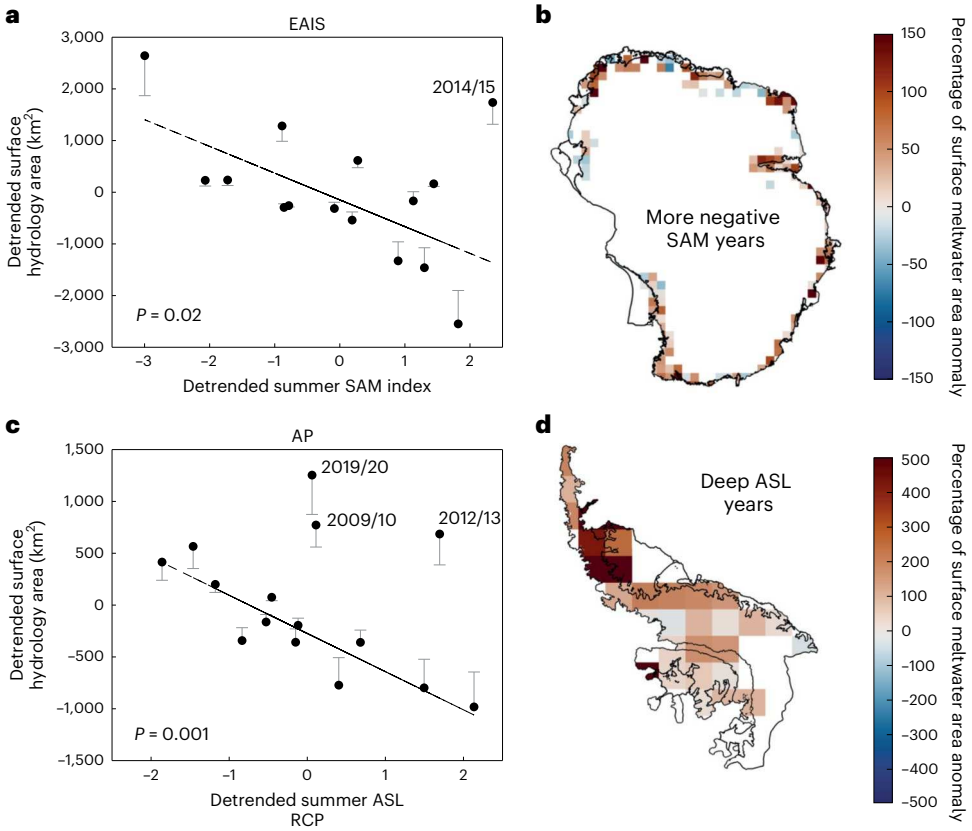

Fig. 4 | Links between Antarctic surface meltwater and climate for the EAIS and AP. a, Significant ($P < 0.05$) negative relationship (linear regression) between surface meltwater area and the summer SAM index for the EAIS (black dots, with grey bars extending to observed meltwater area), with regression (black line) shown ($P = 0.02$). **b**, Surface meltwater area anomalies across the EAIS in years with summer SAM < 0.7, showing widespread positive anomalies of >50%. **c**, Significant negative relationship between surface meltwater and ASL RCP on the AP ($P = 0.001$). The melt seasons of three distinct outliers with higher-than-expected surface meltwater are labelled. **d**, High percentage surface meltwater anomalies on the AP during years with ASL RCP <−8 (deep ASL years). Ice-sheet and ice-shelf boundaries in **b** and **d** from ref. 56.

centre of the ASL is closer to the AP (Extended Data Figs. 4h and 6c,d), consistent with the correlation to wind and temperature[28]. While ASL strength has a distinct broad-scale influence on AP surface meltwater, the three highest meltwater years (09/10, 12/13 and 19/20) stand out as clear outliers to this relationship (Fig. 4c). These years did not have exceptionally eastward ASL longitudes (Extended Data Table 2), suggesting that local feedbacks and variability in surface meteorological conditions, and extreme weather events, are important in controlling the most intense melt events[32,33]. We do not observe statistically significant relationships between surface meltwater area and either SAM or ENSO on the AP (Extended Data Fig. 4e,f), perhaps due to the known dependency of AP temperatures on the combined impact of ENSO and the SAM[34], weaker ENSO links in austral summer to AP temperatures[34] and/or links between the eastern AP and tropical climate variability in other regions[35]. No statistically significant relationships are observed for the WAIS (Extended Data Fig. 4i–l), possibly due to meltwater area being too low for discernable signals to be identified.

We find positive significant power law relationships between monthly surface meltwater area and modelled snowmelt for both the EAIS ($R^2 = 0.37$, $P < 0.01$) and the WAIS ($R^2 = 0.60$, $P < 0.01$) (Fig. 5a). Perhaps surprisingly, given the large area difference between the ice sheets, the magnitude of monthly modelled snowmelt integrated across the EAIS is only 43% higher on average than for the WAIS. However, the amount of snowmelt that becomes ponded surface meltwater is one-to-two orders of magnitude greater for the EAIS than the WAIS (Fig. 5a). Hence, at an ice-sheet scale, melting in East Antarctica results in a proportionally far greater increase in surface meltwater area than in West Antarctica. For the EAIS, meltwater area increases at a greater rate than modelled melt across our study period, indicating increasing susceptibility of melt to pond on the ice surface. This increase is observed at both ice-sheet-wide and ice-shelf scales across the EAIS (Fig. 6). During the first half of our study period, relatively high cumulative modelled snowmelt totals (November–February sum) in 2009/10 (74 Gt), 2010/11 (66 Gt) and 2012/13 (89 Gt) translated into peak monthly surface meltwater areas of ~1,000–1,800 km² (Fig. 5b). By contrast, modelled snowmelt totals of a similar magnitude in 2013/14 (83 Gt), 2016/17 (79 Gt) and 2019/20 (91 Gt) coincided with total surface meltwater area of ~2,900–4,500 km² (Fig. 5b). At a regional scale, 14 out of 17 analysed EAIS ice-shelf regions show increasing surface meltwater area relative to modelled melt, seven of which show statistically significant trends across our study period (Fig. 6a–g). These include Shackleton and Nivlisen ice shelves, the third and fourth highest contributors to total meltwater area in East Antarctica.

At the AP, we observe hysteresis rather than a power law relationship between modelled melt and meltwater area, with surface meltwater area lagging behind modelled snowmelt (Fig. 5a). Relatively high snowmelt in December typically coincides with total meltwater areas of 5–100 km², whereas surface meltwater areas of 300–800 km² in February occur with less snowmelt. While a similar lag effect is observed for the EAIS and WAIS, these signals are less pronounced (Fig. 5a). There is far greater variability in AP surface meltwater area values relative to the same magnitude of melt than is observed for either the EAIS or WAIS. No clear patterns in ice-shelf susceptibility to melt were identified for the AP or WAIS.

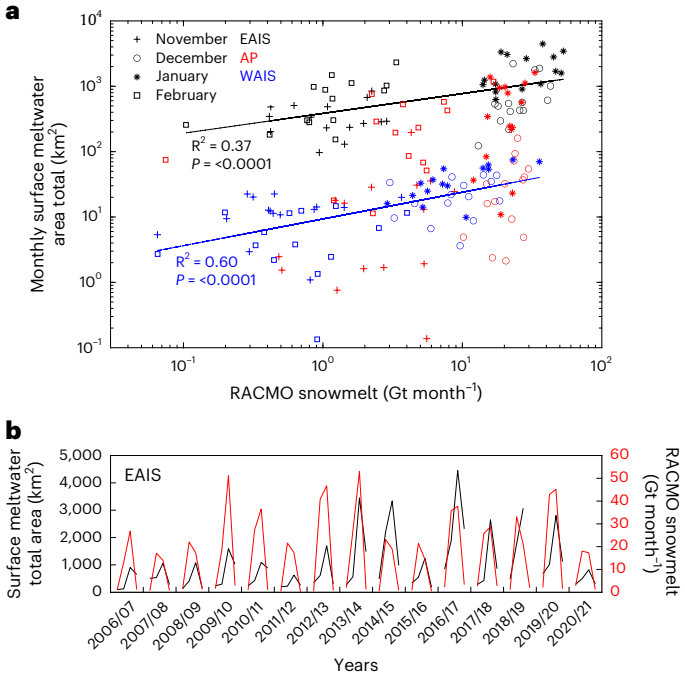

Fig. 5 | Comparison between surface meltwater area and modelled snowmelt. **a**, The relationship between monthly surface meltwater area and monthly RACMO modelled snowmelt, integrated across the EAIS (black), WAIS (blue) and AP (red). Statistically significant ($P < 0.05$) results from linear regression are displayed for the EAIS ($P = 2.8 \times 10^{-5}$) and WAIS ($P = 7.5 \times 10^{-13}$). The different symbols indicate the month (November–February) of each data point. **b**, Time series of surface meltwater area (black) and modelled snowmelt (red) across the EAIS, for the months of November–February each melt season.

Discussion

The likelihood of surface meltwater being able to pond on an ice surface is primarily controlled by the balance between snow accumulation and snowmelt[36]. Thicker snowpacks have a greater capacity for holding meltwater, meaning more melt is required to saturate the pore space and trigger surface ponding. This could explain the lagged effect on the AP (Fig. 5a), where high accumulation rates[30] result in thick snowpacks, which take time to saturate with meltwater before ponding can occur. Despite having only marginally higher ice-sheet-wide integrated modelled melt rates, the EAIS hosts substantially more surface meltwater (Fig. 5a) than the WAIS, suggesting that, in general, WAIS snowpacks are currently less susceptible to meltwater saturation and surface ponding.

Our results show an overall increase in the magnitude and variability of surface meltwater area across the EAIS throughout our study period, despite ice-sheet-wide modelled snowmelt rates remaining relatively consistent (Fig. 5b). Regional analysis suggests that this increased sensitivity to meltwater ponding has occurred around the entire EAIS margin, but has been most pronounced at ice shelves in Dronning Maud Land and Wilkes Land (Fig. 6a). While there are several climatic and glaciological controls that could explain this increased sensitivity, we hypothesize that the cause was an increase in the abundance of low permeability ice surfaces in East Antarctica. Reduced ice-sheet surface permeability can occur for several reasons: enhanced wind scouring exposing ice surfaces[14,37]; multi-annual melting and freezing of water within the snowpack forming impermeable ice lenses[38,39]; and reductions in firn air content due to reduced accumulation or the snowpack becoming saturated with melt[40,41]. These processes have already been observed at regional scales in Antarctica[18,38], and have resulted in widespread reductions in permeability across the Greenland ice sheet[42]. Our results suggest that a similar effect may be occurring in East Antarctica, although detailed analysis of in situ, modelled and satellite data would be required to assess the specific surface conditions for any given location. High variability in meltwater area (sometimes despite similar magnitudes of melt; Fig. 6b–h) between different EAIS ice shelves suggests strong regional variability in susceptibility to meltwater ponding, probably due to regional differences in firn thickness and saturation.

The associations between surface meltwater area and the SAM in East Antarctica, and the ASL on the AP, demonstrate the broad-scale influence that these modes of climate variability can have on melt[43]. At the AP, a deeper (lower pressure) ASL typically brings relatively warm, northerly air flows down the western side of the AP[34], enhancing surface air temperature and the likelihood of melting[44]. At the EAIS, the negative correlation between the SAM and surface meltwater area is consistent with the known influence of the SAM on EAIS surface air temperatures[29,43] and observed relationships between surface air temperature and meltwater ponding[18]. Extreme melt years that cannot be explained by these drivers may be related to localized factors, such as solar radiation[44,45], foehn winds[45,46] and low cloud cover[47], or to extreme weather events, often driven by atmospheric rivers[48]. Although related to large-scale drivers, atmospheric rivers often have quite specific configurations[32], which would not be detected by our correlation or composite analysis.

The presence of surface meltwater ponds can provide sufficient meltwater supply to initiate hydrofracture, either on floating[49,50] or grounded ice[7,51]. While most ice-shelf regions which currently host surface meltwater are thought to be resilient to hydrofracture[50], overall increases in surface meltwater area could result in expansion into more vulnerable areas, as has already been observed at Shackleton Ice Shelf[18]. The proportion of Antarctic ice shelves that are currently covered in surface meltwater is low (Extended Data Fig. 1), and future anticipated increases in melt[52] may partly be mitigated by increased evacuation of meltwater off ice shelves[53]. Increases in surface meltwater on grounded ice would increase the likelihood of surface-to-bed connections developing, which could limit the amount of meltwater that drains from the ice sheet onto ice shelves. However, the delivery of surface meltwater to the bed could have important implications for grounded ice dynamics, as it can induce transient[7] and seasonal[54,55] accelerations in ice motion.

Methodological advances and computing capabilities have enabled us to produce a monthly, continent-wide dataset of Antarctic surface meltwater area for 2006–2021. Our results show that there has been an increase in the magnitude and variability of surface meltwater area in East Antarctica in recent years, which, in the absence of a coincident increase in modelled snowmelt, suggests that the ice-sheet surface is becoming increasingly prone to meltwater ponding. These results create an imperative for our surface meltwater dataset to be combined with modelled, satellite and in situ data, to better understand the controls and potential future impacts of meltwater ponding in regions most at risk to increases in surface meltwater area.

Online content

Any methods, additional references, Nature Portfolio reporting summaries, source data, extended data, supplementary information, acknowledgements, peer review information; details of author contributions and competing interests; and statements of data and code availability are available at https://doi.org/10.1038/s41558-025-02363-5.

References

1. Scambos, T. A., Hulbe, C., Fahnestock, M. & Bohlander, J. The link between climate warming and break-up of ice shelves in the Antarctic peninsula. *J. Glaciol.* **46**, 516–530 (2000).
2. Banwell, A. F., MacAyeal, D. R. & Sergienko, O. V. Breakup of the Larsen B ice shelf triggered by chain reaction drainage of supraglacial lakes. *Geophys. Res. Lett.* **40**, 5872–5876 (2013).

https://doi.org/10.1038/s41558-025-02363-5

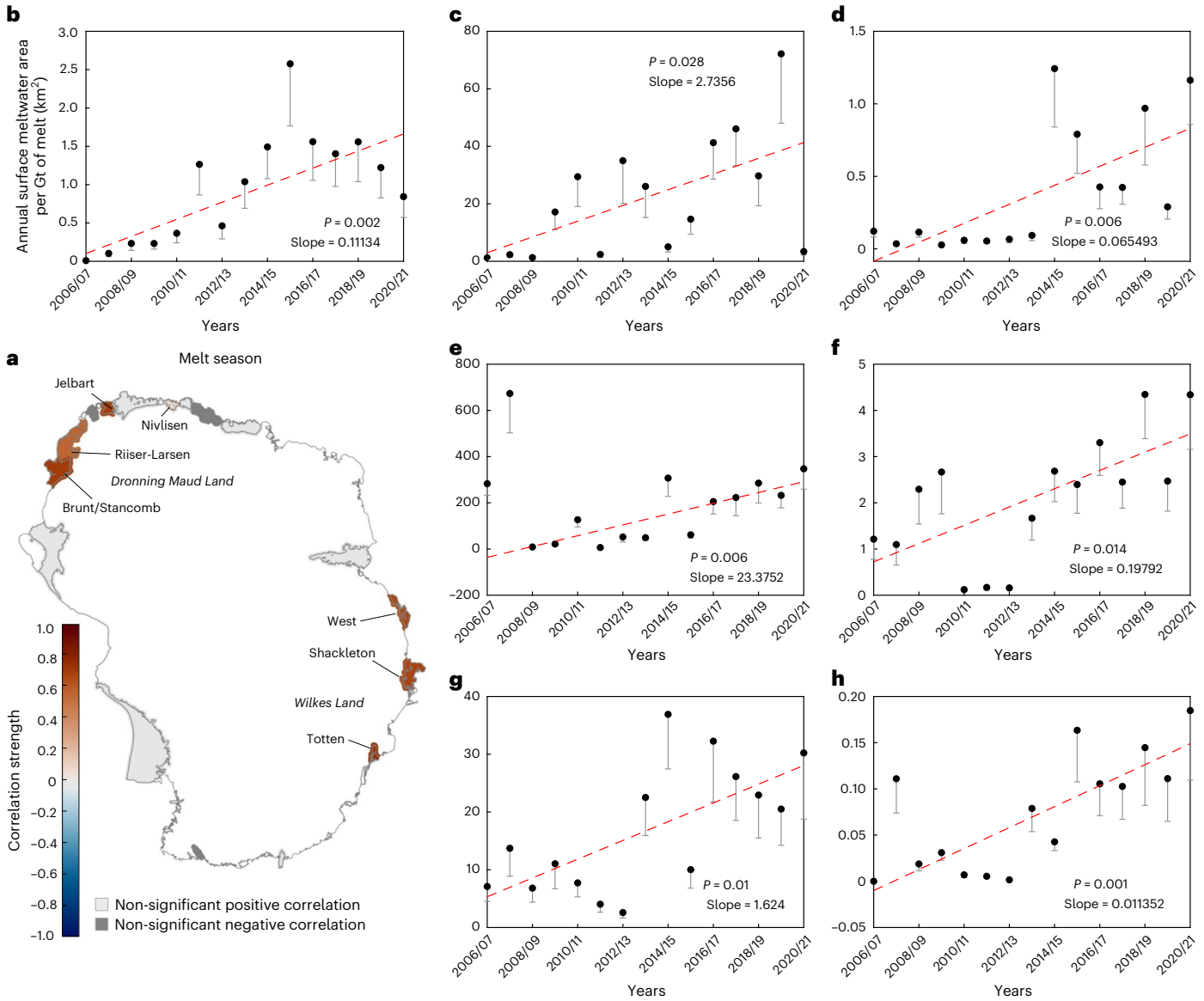

Fig. 6 | Increasing sensitivity of East Antarctic ice-shelf regions to surface meltwater ponding. a, Map indicating the correlation strength between time (years since start of study period) and surface meltwater ponding susceptibility (quantified as annual surface meltwater area per unit Gt of modelled melt) for selected ice shelves around East Antarctica. The correlation strengths of ice-shelf regions with statistically significant relationships are displayed on a red–blue divergent colour-scale, with non-significant ice shelves shaded in light (positive correlation) or dark (negative) grey. **b**–**h**, Scatter plots for ice shelves labelled in **a**, which display a statistically significant increasing trend (linear regression) in meltwater ponding susceptibility throughout our study period: Brunt/Stancomb (**b**), Riiser-Larsen (**c**), Jelbart (**d**), Nivlisen (**e**), West (**f**), Shackleton (**g**) and Totten (**h**). Grey bars indicate the difference in result if using observed meltwater area. Note the large differences in *y* axis scale between plots. Ice-sheet and ice-shelf boundaries in **a** from ref. 56.

3. Kingslake, J., Ely, J. C., Das, I. & Bell, R. E. Widespread movement of meltwater onto and across Antarctic ice shelves. *Nature* **544**, 349–352 (2017).
4. Jakobs, C. L., Reijmer, C. H., van den Broeke, M. R., van de Berg, W. J. & van Wessem, J. M. Spatial variability of the snowmelt-albedo feedback in Antarctica. *J. Geophys. Res. Earth Surf.* **126**, e2020JF005696 (2021).
5. Zwally, H. J. et al. Surface melt-induced acceleration of Greenland ice-sheet flow. *Science* **297**, 218–222 (2002).
6. Bell, R. E., Banwell, A. F., Trusel, L. D. & Kingslake, J. Antarctic surface hydrology and impacts on ice-sheet mass balance. *Nat. Clim. Change* **8**, 1044–1052 (2018).
7. Tuckett, P. A. et al. Rapid accelerations of Antarctic peninsula outlet glaciers driven by surface melt. *Nat. Commun.* **10**, 4311 (2019).
8. David, T. W. E. & Priestley, R. E. *Geological Observations in Antarctica by the British Antarctic Expedition 1907–1909* (JP Lippincott, 1909).
9. Reynolds, J. M. Lakes on George VI ice shelf, Antarctica. *Polar Rec.* **20**, 425–432 (1981).
10. Phillips, H. A. Surface meltstreams on the Amery ice shelf, east Antarctica. *Ann. Glaciol.* **27**, 177–181 (1998).
11. Stokes, C. R., Sanderson, J. E., Miles, B. W. J., Jamieson, S. S. R. & Leeson, A. A. Widespread distribution of supraglacial lakes around the margin of the east Antarctic ice sheet. *Sci. Rep.* **9**, 13823 (2019).
12. Arthur, J. F., Stokes, C. R., Jamieson, S. S. R., Carr, J. R. & Leeson, A. A. Distribution and seasonal evolution of supraglacial lakes on Shackleton ice shelf, east Antarctica. *Cryosphere* **14**, 4103–4120 (2020).

13. Dell, R. et al. Lateral meltwater transfer across an Antarctic ice shelf. *Cryosphere* **14**, 2313–2330 (2020).
14. Tuckett, P. A. et al. Automated mapping of the seasonal evolution of surface meltwater and its links to climate on the Amery ice shelf, Antarctica. *Cryosphere* **15**, 5785–5804 (2021).
15. Moussavi, M. et al. Antarctic supraglacial lake detection using Landsat 8 and Sentinel-2 imagery: towards continental generation of lake volumes. *Remote Sens.* **12**, 134 (2020).
16. Dirscherl, M. C., Dietz, A. J. & Kuenzer, C. Seasonal evolution of Antarctic supraglacial lakes in 2015–2021 and links to environmental controls. *Cryosphere* **15**, 5205–5226 (2021).
17. Corr, D., Leeson, A., McMillan, M., Zhang, C. & Barnes, T. An inventory of supraglacial lakes and channels across the west Antarctic ice sheet. *Earth Syst. Sci. Data* **14**, 209–228 (2022).
18. Arthur, J. F. et al. Large interannual variability in supraglacial lakes around east Antarctica. *Nat. Commun.* **13**, 1711 (2022).
19. Trusel, L. D., Frey, K. E., Das, S. B., Munneke, P. K. & van den Broeke, M. R. Satellite-based estimates of Antarctic surface meltwater fluxes. *Geophys. Res. Lett.* **40**, 6148–6153 (2013).
20. Johnson, A., Hock, R. & Fahnestock, M. Spatial variability and regional trends of Antarctic ice shelf surface melt duration over 1979–2020 derived from passive microwave data. *J. Glaciol.* **68**, 533–546 (2022).
21. Banwell, A. F., Wever, N., Dunmire, D. & Picard, G. Quantifying Antarctic-wide ice-shelf surface melt volume using microwave and firn model data: 1980 to 2021. *Geophys. Res. Lett.* **50**, e2023GL102744 (2023).
22. Kuipers Munneke, P., Picard, G., van den Broeke, M. R., Lenaerts, J. T. M. & van Meijgaard, E. Insignificant change in Antarctic snowmelt volume since 1979. *Geophys. Res. Lett.* **39**, L01501 (2012).
23. van Wessem, J. M. et al. Modelling the climate and surface mass balance of polar ice sheets using RACMO2—Part 2: Antarctica (1979–2016). *Cryosphere* **12**, 1479–1498 (2018).
24. Arthur, J. F., Stokes, C., Jamieson, S. S., Carr, J. R. & Leeson, A. A. Recent understanding of Antarctic supraglacial lakes using satellite remote sensing. *Prog. Phys. Geogr.* **44**, 837–869 (2020).
25. Nicolas, J. P. et al. January 2016 extensive summer melt in west Antarctica favoured by strong El Niño. *Nat. Commun.* **8**, 15799 (2017).
26. Banwell, A. F. et al. The 32-year record-high surface melt in 2019/2020 on the northern George VI ice shelf, Antarctic peninsula. *Cryosphere* **15**, 909–925 (2021).
27. Fogt, R. L., Bromwich, D. H. & Hines, K. M. Understanding the SAM influence on the South Pacific ENSO teleconnection. *Clim. Dynam.* **36**, 1555–1576 (2011).
28. Raphael, M. N. et al. The Amundsen sea low: variability, change, and Impact on Antarctic climate. *Bull. Am. Meteorol. Soc.* **97**, 111–121 (2016).
29. Fogt, R. L. & Marshall, G. J. The southern annular mode: variability, trends, and climate impacts across the Southern Hemisphere. *WIREs Clim. Change* **11**, e652 (2020).
30. Noël, B. et al. Higher Antarctic ice sheet accumulation and surface melt rates revealed at 2 km resolution. *Nat. Commun.* **14**, 7949 (2023).
31. Hosking, J. S., Orr, A., Marshall, G. J., Turner, J. & Phillips, T. The influence of the Amundsen–Bellingshausen seas low on the climate of west Antarctica and its representation in coupled climate model simulations. *J. Clim.* **26**, 6633–6648 (2013).
32. Gorodetskaya, I. V. et al. Record-high Antarctic peninsula temperatures and surface melt in February 2022: a compound event with an intense atmospheric river. *Npj Clim. Atmos. Sci.* **6**, 202 (2023).
33. Siegert, M. J. et al. Antarctic extreme events. *Front. Environ. Sci.* **11**, 1229283 (2023).
34. Clem, K. R., Renwick, J. A., McGregor, J. & Fogt, R. L. The relative influence of ENSO and SAM on Antarctic peninsula climate. *J. Geophys. Res. Atmos.* **121**, 9324–9341 (2016).
35. Clem, K. R., Bozkurt, D., Kennett, D., King, J. C. & Turner, J. Central tropical Pacific convection drives extreme high temperatures and surface melt on the Larsen C ice shelf, Antarctic peninsula. *Nat. Commun.* **13**, 3906 (2022).
36. van Wessem, J. M., van den Broeke, M. R., Wouters, B. & Lhermitte, S. Variable temperature thresholds of melt pond formation on Antarctic ice shelves. *Nat. Clim. Change* **13**, 161–166 (2023).
37. Lenaerts, J. T. M. et al. Meltwater produced by wind–albedo interaction stored in an east Antarctic ice shelf. *Nat. Clim. Change* **7**, 58–62 (2017).
38. Hubbard, B. et al. Massive subsurface ice formed by refreezing of ice-shelf melt ponds. *Nat. Commun.* **7**, 11897 (2016).
39. Buzzard, S., Feltham, D. & Flocco, D. Modelling the fate of surface melt on the Larsen C ice shelf. *Cryosphere* **12**, 3565–3575 (2018).
40. Ligtenberg, S. R. M., Kuipers Munneke, P. & van den Broeke, M. R. Present and future variations in Antarctic firn air content. *Cryosphere* **8**, 1711–1723 (2014).
41. Munneke, P. K., Ligtenberg, S. R. M., Broeke, M. R. V. D. & Vaughan, D. G. Firn air depletion as a precursor of Antarctic ice-shelf collapse. *J. Glaciol.* **60**, 205–214 (2014).
42. MacFerrin, M. et al. Rapid expansion of Greenland's low-permeability ice slabs. *Nature* **573**, 403–407 (2019).
43. Orr, A. et al. Characteristics of surface 'melt potential' over Antarctic ice shelves based on regional atmospheric model simulations of summer air temperature extremes from 1979/80 to 2018/19. *J. Clim.* **36**, 3357–3383 (2023).
44. Gilbert, E., Orr, A., Renfrew, I. A., King, J. C. & Lachlan-Cope, T. A 20-year study of melt processes over Larsen C ice shelf using a high-resolution regional atmospheric model: 2. Drivers of surface melting. *J. Geophys. Res. Atmos.* **127**, e2021JD036012 (2022).
45. Elvidge, A. D., Kuipers Munneke, P., King, J. C., Renfrew, I. A. & Gilbert, E. Atmospheric frivers of melt on Larsen C ice shelf: surface energy budget regimes and the impact of foehn. *J. Geophys. Res. Atmos.* **125**, e2020JD032463 (2020).
46. King, J. C. et al. The impact of föhn winds on surface energy balance during the 2010–2011 melt season over Larsen C ice shelf, Antarctica. *J. Geophys. Res. Atmos.* **122**, 12062–12076 (2017).
47. Gilbert, E. et al. Summertime cloud phase strongly influences surface melting on the Larsen C ice shelf, Antarctica. *Q. J. R. Meteorol. Soc.* **146**, 1575–1589 (2020).
48. Wille, J. D. et al. Antarctic atmospheric river climatology and precipitation impacts. *J. Geophys. Res. Atmos.* **126**, e2020JD033788 (2021).
49. Scambos, T. et al. Ice shelf disintegration by plate bending and hydro-fracture: satellite observations and model results of the 2008 Wilkins ice shelf break-ups. *Earth Planet. Sci. Lett.* **280**, 51–60 (2009).
50. Lai, C.-Y. et al. Vulnerability of Antarctica's ice shelves to meltwater-driven fracture. *Nature* **584**, 574–578 (2020).
51. Das, S. B. et al. Fracture propagation to the base of the Greenland ice sheet during supraglacial lake drainage. *Science* **320**, 778–781 (2008).
52. Trusel, L. D. et al. Divergent trajectories of Antarctic surface melt under two twenty-first-century climate scenarios. *Nat. Geosci.* **8**, 927–932 (2015).
53. Bell, R. E. et al. Antarctic ice shelf potentially stabilized by export of meltwater in surface river. *Nature* **544**, 344–348 (2017).

54. Boxall, K., Christie, F. D. W., Willis, I. C., Wuite, J. & Nagler, T. Seasonal land-ice-flow variability in the Antarctic peninsula. *Cryosphere* **16**, 3907–3932 (2022).
55. Wallis, B. J., Hogg, A. E., van Wessem, J. M., Davison, B. J. & van den Broeke, M. R. Widespread seasonal speed-up of west Antarctic peninsula glaciers from 2014 to 2021. *Nat. Geosci.* **16**, 231–237 (2023).
56. Mouginot, J., Scheuchl, B. & Rignot, E. MEaSUREs Antarctic Boundaries for IPY 2007–2009 from Satellite Radar, Version 2 [Dataset] (NASA National Snow and Ice Data Center Distributed Active Archive Center, 2017); https://doi.org/10.5067/AXE4121732AD

Methods

Surface meltwater mapping

Surface meltwater, ice, rock and cloud were automatically detected from Landsat 7 and 8 optical satellite imagery using a band-thresholding technique[15]. Cloud and rock areas were masked from image tiles, and an ice-specific version of the normalized difference water index ($NDWI_{ice}$) was subsequently used to delineate areas of surface meltwater. We applied the same thresholds as those developed by ref. 15, except for one minor change; we altered the threshold value for 'green (B3)−red (B4)' from >0.07 to >0.10 (Supplementary Table 3). This threshold is applied following NDWI classification to exclude areas of cloud shadow and shaded snow from surface meltwater classification results[15]. Our testing found that a threshold of >0.07 was insufficient at removing all rock and cloud shadow, resulting in widespread instances of misclassification error (Supplementary Fig. 4). By increasing this threshold to >0.10, we were able to successfully eradicate these misclassifications, while still retaining correctly identified surface meltwater within our dataset (Supplementary Discussion 3).

Mapping was undertaken in GEE, using Landsat level 1 tier 2 top-of-atmosphere images stored in the GEE data catalogue. By using a cloud-based computational platform, we were able to conduct rapid processing over spatial and temporal scales that would have otherwise been unachievable[14]. Surface meltwater was mapped monthly between 2006 and 2021. Before 2006, image coverage was insufficient to generate comprehensive continent-wide data. Only images that had a sun elevation angle >20° were processed[15], hence limiting surface meltwater data to austral summer months. This filtering step was taken to avoid misclassification errors, since surface water is difficult to differentiate spectrally in low-light conditions[57]. Surface meltwater is rare outside austral summer months regardless[58]. Our mapping procedure incorporated a robust method for assessing image visibility, enabling us to quantify variability in image coverage and cloud cover[14]. Using this approach, we estimated the maximum area of surface hydrology that would be expected under cloud-free conditions[14], in addition to the observed mapped values. A discussion of the uncertainties associated with this method are provided in Supplementary Discussion 1. We mapped both monthly and 'annual' (November–February, to cover the melt season) maximum area of surface meltwater, for ease of comparison with climate datasets.

A total area of ~12.32 million km^2 was covered during surface meltwater mapping, including both the grounded ice sheet and surrounding ice shelves. Every Landsat image covering this study area between 2006 and 2021 was used during analysis, totalling 133,497 images. Our mapping procedure involved automatically looping through an Antarctic-wide grid of 1,151 region-of-interest (ROI) shapefile tiles, ordinarily 108 × 108 km^2 in area. This tile size maximized spatial coverage for mapping, while remaining within the memory capacity of an individual task within GEE. Landsat image coverage does not extend to latitudes greater than ~85° south; hence ROI tiles that overlapped this area (~1.28 million km^2) were not mapped (Fig. 1). However, given the high elevation and very low temperature of the region around the South Pole, little meltwater ever exists at this location. The grid was clipped to the Antarctic coastline[56,59], meaning coastal ROI tiles varied in shape and area. We did not account for changes in ice-shelf area throughout our study period. Our results show that surface meltwater rarely ponds adjacent to ice shelf calving fronts (it typically exists further inland near the grounding line); hence we deemed that minor changes in ice-shelf area will have had negligible influence on mapped meltwater totals. Tiles were given a unique ID based on longitude and latitude for identification purposes. In instances where the coastline clipping process split a tile into multiple portions, tile segments were merged to adjacent tiles to ensure no two tiles had the same ID.

Processing was performed on a yearly basis for up to ~350 ROI tiles at a time. Memory capacity and timeout limits within GEE were exceeded when attempting to process larger regions than this. Following the method of ref. 14, vector outputs were exported from GEE as geoJSON files. Post-processing steps were then undertaken in MATLAB to clean the raw data and to produce final shapefile outputs. For full details of the lake detection, image visibility assessment and post-processing methods applied here, see ref. 14.

Surface meltwater quality control

Surface meltwater quality control was conducted to identify any artifacts within the continent-wide dataset. Annual maximum extent surface meltwater shapefiles were merged to produce a single continent-wide map. Quality control was then performed via manual inspection of this 15-yr maximum extent raster layer (Extended Data Fig. 7), as this offered the quickest method for flagging invalid meltwater polygons. Polygons that (1) existed in highly improbable locations (for example, at high elevations in the cold interior of the ice sheet), (2) had straight or cornered edges or (3) formed an ordered or repeated pattern were searched for during manual inspection. Polygons that satisfied some or all of the above criteria were highlighted for verification and checked against the optical images from which they originated. In all cases highlighted by the above process, flagged lake polygons were the result of artifacts in Landsat 7 imagery and were removed from the final dataset. In total, 699 polygons were removed during this process, totalling 9.87 km^2 of incorrectly identified meltwater area.

Owing to the large spatial and temporal scale of our study, it was not realistic to conduct systematic manual verification of each individually mapped instance of surface meltwater against its corresponding optical imagery. The thresholds we applied to delineate surface meltwater, modified from ref. 15, were established on the basis of a range of spectral conditions around Antarctica. Their verification against optical imagery showed an accuracy of >95% (ref. 15) and mapped outputs showed high similarity with meltwater area data produced by alternative methods[57]. Our minor adjustment to their method (Supplementary Discussion 3) reduces the likelihood of cloud and rock shadow misclassifications, providing further confidence in the accuracy of our meltwater classifications. Furthermore, ref. 14 showed that the thresholds were suitable for use on both Landsat 7 and 8 imagery (Supplementary Discussion 4). It should be noted that our dataset only captures surface meltwater identifiable in the visible spectrum and cannot be used to make conclusions about melt rates or subsurface meltwater storage. The 30-m resolution of Landsat additionally means that we will not have captured the smallest-scale surface meltwater features, such as streams or small lakes. Areas of slush (which are particularly common on ice shelves and sections of grounded ice on the northern AP, Extended Data Fig. 2g,h) identified by the thresholds have been retained within the dataset. However, while our dataset contains some areas of slush, the thresholds we applied were designed specifically for mapping surface meltwater (not slush); hence, alternative methods[60,61] would be required to comprehensibly map slush across Antarctica.

While systematic method performance was not assessed, sample mapped results were visually compared against optical imagery when trialling our method in different regions of Antarctica. Overall, the thresholds were extremely effective at identifying surface meltwater across all regions of Antarctica, with <1% of mapped meltwater pixels identified as misclassification error based on 100 randomly sampled features across Antarctica. Errors were highest in regions with dirty ice (such as McMurdo Ice Shelf), high crevasse shadow or variable slush presence (Extended Data Fig. 2). However, misclassified meltwater features were typically small (<5 pixels in size) and limited in spatial extent, and were therefore deemed to have minimal influence on regional or ice-sheet scale results (Supplementary Discussion 5). On the basis of all the stated reasons, we hence considered the method to be sufficiently accurate for continent-wide application, without needing to adjust thresholds for different regions.

Statistical analyses

We generated regional surface meltwater area totals by aggregating mapped meltwater areas across the EAIS, WAIS and AP, and for individual ice shelves and their associated grounding zones. Ice-sheet scale (EAIS, WAIS and AP) and ice-shelf regions were defined using basins from ref. 59. Grounded catchments and ice shelves were merged in ArcMap on the basis of their ice-sheet classification, to produce polygons for the EAIS, WAIS and AP. Ice-shelf regions included the ice shelf as defined by ref. 59 plus a 20-km buffer onto grounded ice inland from the grounding line. We took this additional step to ensure that surface meltwater in the grounding zone of an ice shelf, where it is typically most abundant[7], was included in regional analysis.

We assessed changes in meltwater area over time using robust linear regression in MATLAB (https://uk.mathworks.com/help/stats/robustfit.html). Our data are unusual in that we only have data during 4 months of the year; hence we have repeated seasonal gaps in our time series. Regression analyses, using time as the independent variable, were therefore used instead of traditional trend analysis techniques (such as the Mann–Kendall test), which require data to have no serial correlation or seasonality. Data were tested to check that they met the assumptions of robust linear regression. Robust regression is less sensitive to outliers than standard linear regression, allowing us to test for the presence of broad-scale trends across our study period, without being disproportionally skewed by one or two outlier years. Regression analyses were performed on individual monthly surface meltwater area data (November–February) and on annual maximum extent data (Extended Data Fig. 3). Analyses were run on both our mapped and estimated meltwater area data, to investigate how the results varied (Supplementary Discussion 2). Standardized *Z*-scores of annual surface meltwater area totals were additionally calculated in MATLAB, enabling quantification of surface meltwater area for individual years relative to the study period mean (Fig. 3).

Comparison with climate data

Climatic indices for three modes of Antarctic climate variability were compared against our surface meltwater area data: (1) the SAM index, from the observation-based index following ref. 62; (2) the Oceanic Niño index, one measure for the ENSO, from the National Oceanic and Atmospheric Administration (NOAA); and (3) ASL indices of RCP and longitude, following ref. 63. RCP data were used in preference to 'actual' central pressure data to isolate changes in the ASL from the SAM, which strongly modulates the actual pressure across all seasons[29]. Each climate index provides a simple diagnostic quantity, which is used to characterize the state of the geophysical system in question. For all the datasets, monthly index values for December, January and February were averaged to generate single, austral summer values. These 'annual' values were then compared against the annual maximum extent of surface meltwater. Climatic and surface meltwater data were detrended before conducting robust regression analysis, which enabled us to better assess the statistical relationship for each individual mode of climatic variability, without results being skewed by anonymously high- or low-melt years, which could have been strongly influenced via teleconnections with other climatic modes[64].

We performed composite analysis[29,65], a commonly used statistical technique to identify potential impacts of climatic phenomena, to explore the large-scale impact of modes of climatic variability on surface meltwater area. For each climatic mode, we determined thresholds to categorize subsets of 'low' and 'high' yearly values. Thresholds were chosen on the basis of visual inspection of plotted time series for each climatic index, with thresholds selected to separate clear 'peaks' and 'troughs' in the data. We produced composite surface meltwater fields for each category by averaging the surface meltwater totals for each subset of years. Mean surface meltwater area totals were calculated on a tile-by-tile basis, using the Antarctic-wide grid used during mapping.

RACMO comparison

We compared our meltwater area data to a statistically downscaled version[30] (2-km resolution) of the regional climate model RACMO2.3.p2 (ref. 23). Reference 30 produced this statistically downscaled product by refining the spatial distribution of surface mass balance components using high-resolution (2 km) datasets, including the reference elevation model of Antarctica (REMA) and an albedo map from the moderate resolution imaging spectroradiometer (MODIS). These data therefore offer higher spatial resolution estimates of meltwater production than previous modelled datasets and are shown to have closer agreement with in situ and satellite records[30]. Monthly meltwater totals were integrated across each respective ice-sheet area to produce monthly totals of meltwater production for the EAIS, WAIS and AP (Fig. 5). We additionally compared RACMO snowmelt against surface meltwater area for each individual ice-shelf region (Fig. 6) and each ROI tile used during mapping, to assess spatial variability in agreement between the two datasets. For any tile where meltwater was mapped in at least 5 months throughout the study period, we correlated monthly meltwater area against RACMO snowmelt (Extended Data Fig. 8).

Data availability

Surface meltwater outputs are available via Zenodo at https://doi.org/10.5281/zenodo.14865075 (ref. 66). Landsat imagery is freely available via the GEE data catalogue (https://developers.google.com/earth-engine/datasets/catalog/landsat). The Landsat Image Mosaic of Antarctica is freely available from the US Geological Survey (https://lima.usgs.gov/). SAM index data are available from the British Antarctic Survey (http://www.nerc-bas.ac.uk/public/icd/gjma/newsam.1957.2007.seas.txt). ENSO index data are available from the NOAA (https://origin.cpc.ncep.noaa.gov/products/analysis_monitoring/ensostuff/ONI_v5.php). ASL index data, following ref. 63 are available at https://scotthosking.com/asl_index. Statistically downscaled RACMO2.3p2 model data[30] are available upon request from B. Noël (bnoel@uliege.be).

Code availability

The GEE and MATLAB codes for surface meltwater mapping are available via Zenodo at https://doi.org/10.5281/zenodo.14866437 (ref. 67).

References

57. Halberstadt, A. R. W. et al. Antarctic supraglacial lake identification using Landsat-8 image classification. *Remote Sens.* **12**, 1327 (2020).
58. Kuipers Munneke, P. et al. Intense winter surface melt on an Antarctic ice shelf. *Geophys. Res. Lett.* **45**, 7615–7623 (2018).
59. Rignot, E., Jacobs, S., Mouginot, J. & Scheuchl, B. Ice-shelf melting around Antarctica. *Science* **341**, 266–270 (2013).
60. Dell, R. L. et al. Supervised classification of slush and ponded water on Antarctic ice shelves using Landsat 8 imagery. *J. Glaciol.* **68**, 401–414 (2022).
61. Dell, R. L., Willis, I. C., Arnold, N. S., Banwell, A. F. & de Roda Husman, S. Substantial contribution of slush to meltwater area across Antarctic ice shelves. *Nat. Geosci.* **17**, 624–630 (2024).
62. Marshall, G. J. Trends in the southern annular mode from observations and reanalyses. *J. Clim.* **16**, 4134–4143 (2003).
63. Hosking, J. S., Orr, A., Bracegirdle, T. J. & Turner, J. Future circulation changes off west Antarctica: sensitivity of the Amundsen sea low to projected anthropogenic forcing. *Geophys. Res. Lett.* **43**, 367–376 (2016).
64. Li, X. et al. Tropical teleconnection impacts on Antarctic climate changes. *Nat. Rev. Earth Environ.* **2**, 680–698 (2021).
65. Marshall, G. J., Di Battista, S., Naik, S. S. & Thamban, M. Analysis of a regional change in the sign of the SAM–temperature relationship in Antarctica. *Clim. Dynam.* **36**, 277–287 (2011).

66. Tuckett, P. A. et al. Antarctic-wide surface meltwater data. *Zenodo* https://doi.org/10.5281/zenodo.14865075 (2025).
67. Tuckett, P. A. et al. Surfmelt_mapping_tool: v1. *Zenodo* https://doi.org/10.5281/zenodo.14866437 (2025).

Acknowledgements

P.A.T. has been supported by a University Post Graduate Research Committee Scholarship from the University of Sheffield. P.A.T. also acknowledges support from the National Environment Research Council (NERC reference NE/X013537/1). J.M.L. acknowledges support from a UKRI Future Leaders Fellowship (grant no. MR/S017232/1 and MR/X02346X/1). E.G. is supported by the PolarRES project, funded by the EU Horizon 2020 programme H2020-LC-CLA-2018-2019-2020 under grant agreement no. 101003590. We thank M. van den Broeke for useful discussions and advice relating to our RACMO comparison and B. Noël for providing the 2-km resolution modelled snowmelt data.

Author contributions

P.A.T., A.J.S., S.J.L. and J.M.L. developed the idea for the paper. P.A.T. developed the surface meltwater mapping methodology, conducted all the analysis and led the paper writing. A.J.S., S.J.L. and J.M.L. provided input on research design and interpretation of results. J.M.J. and E.G. provided guidance on the climate comparison sections. All authors provided input on editing of the paper.

Competing interests

The authors declare no competing interests.

Additional information

Extended data is available for this paper at https://doi.org/10.1038/s41558-025-02363-5.

Supplementary information The online version contains supplementary material available at https://doi.org/10.1038/s41558-025-02363-5.

Correspondence and requests for materials should be addressed to Peter A. Tuckett.

Peer review information *Nature Climate Change* thanks Sarah Thompson and the other, anonymous, reviewer(s) for their contribution to the peer review of this work.

https://doi.org/10.1038/s41558-025-02363-5

Extended Data Table 1 | Surface meltwater area totals on grounded and floating ice per melt season for the Antarctic Ice Sheets

Melt Season	EAIS			AP			WAIS		
	Grounded Area Total (km^2)	Ice Shelf Area Total (km^2)	% Grounded	Grounded Area Total (km^2)	Ice Shelf Area Total (km^2)	% Grounded	Grounded Area Total (km^2)	Ice Shelf Area Total (km^2)	% Grounded
2006/07	546	809	40	29	1135	2	37	29	56
2007/08	832	1165	42	24	251	9	10	8	54
2008/09	697	761	48	17	491	3	17	17	51
2009/10	867	1529	36	15	1465	1	27	30	48
2010/11	629	1400	31	22	799	3	44	39	53
2011/12	463	562	45	10	414	2	43	28	60
2012/13	678	1713	28	36	1469	2	38	67	36
2013/14	1328	2768	32	39	18	68	27	33	45
2014/15	1217	3496	26	31	89	26	47	40	54
2015/16	715	1097	39	250	337	43	38	45	45
2016/17	1796	4149	30	388	383	50	33	42	44
2017/18	1063	2235	32	44	1159	4	24	33	42
2018/19	1547	2698	36	13	45	23	23	39	37
2019/20	1283	2740	32	177	2154	8	31	37	46
2020/21	658	750	47	133	1396	9	23	19	55

All area totals are yearly maximum meltwater area estimates.

https://doi.org/10.1038/s41558-025-02363-5

Extended Data Table 2 | Mean summer climate indices per melt season, alongside corresponding meltwater area totals for the Antarctic Ice Sheets

Melt Season	Climate Indices (Summer mean value)				Meltwater Total Area (km^2)		
	SAM	ENSO	ASL RCP	ASL Longitude (°E)	EAIS	AP	WAIS
2006/07	1.63	0.7	−8.20	233.17	1355	1164	66
2007/08	3.11	−1.6	−6.11	230.75	1997	275	18
2008/09	1.81	−0.8	−7.38	266.33	1457	508	34
2009/10	−0.15	1.5	−6.79	257.33	2396	1480	57
2010/11	0.67	−1.4	−7.41	253.00	2029	821	83
2011/12	2.78	−0.9	−7.16	240.58	1026	424	71
2012/13	0.65	−0.4	−5.37	225.67	2391	1504	105
2013/14	0.5	−0.4	−5.62	203.75	4096	57	60
2014/15	3.69	0.5	−6.76	232.00	4713	120	87
2015/16	2.19	2.5	−8.06	230.83	1811	587	83
2016/17	−1.75	−0.3	−7.39	209.50	5945	771	76
2017/18	2.33	−0.9	−8.51	259.58	3298	1203	57
2018/19	1.43	0.7	−5.25	220.25	4245	58	62
2019/20	−0.96	0.5	−7.37	260.75	4023	2330	68
2020/21	2.88	−1.0	−9.35	246.67	1408	1528	41

Climate index data are displayed for the Southern Annular Mode (SAM), El Niño/Southern Southern Oscillation (ENSO), and Amundsen Sea Low (ASL) Relative Central Pressure (RCP) and Longitude. Mean summer index values are based on the months of December, January and February. Corresponding annual surface meltwater totals for the EAIS, AP and WAIS are also displayed for each melt season.

https://doi.org/10.1038/s41558-025-02363-5

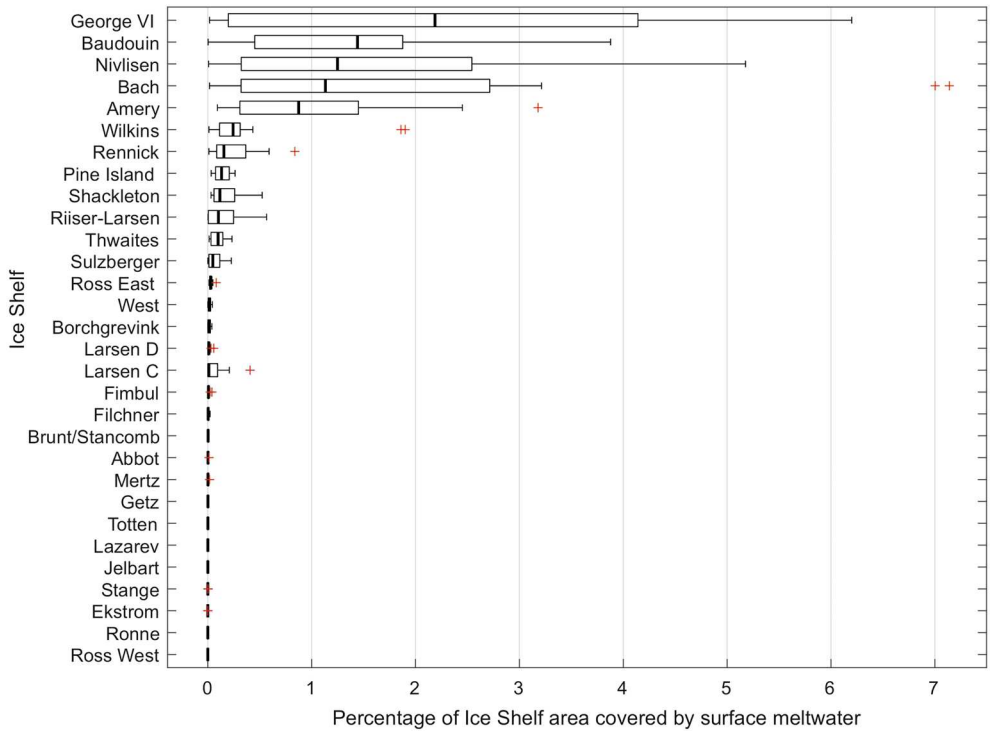

Extended Data Fig. 1 | Variation in percentage meltwater cover for selected Antarctic ice shelves, between 2006 and 2021. Box plots show the median (thick black line), interquartile range (25th and 75th percentiles, indicated by the box ends), and minima/maxima (whiskers) of the data when excluding outliers. Individual outlier points are plotted in red, and are defined as data points greater than 1.5 times the interquartile range from the box. See Fig. 1 for ice shelf locations.

https://doi.org/10.1038/s41558-025-02363-5

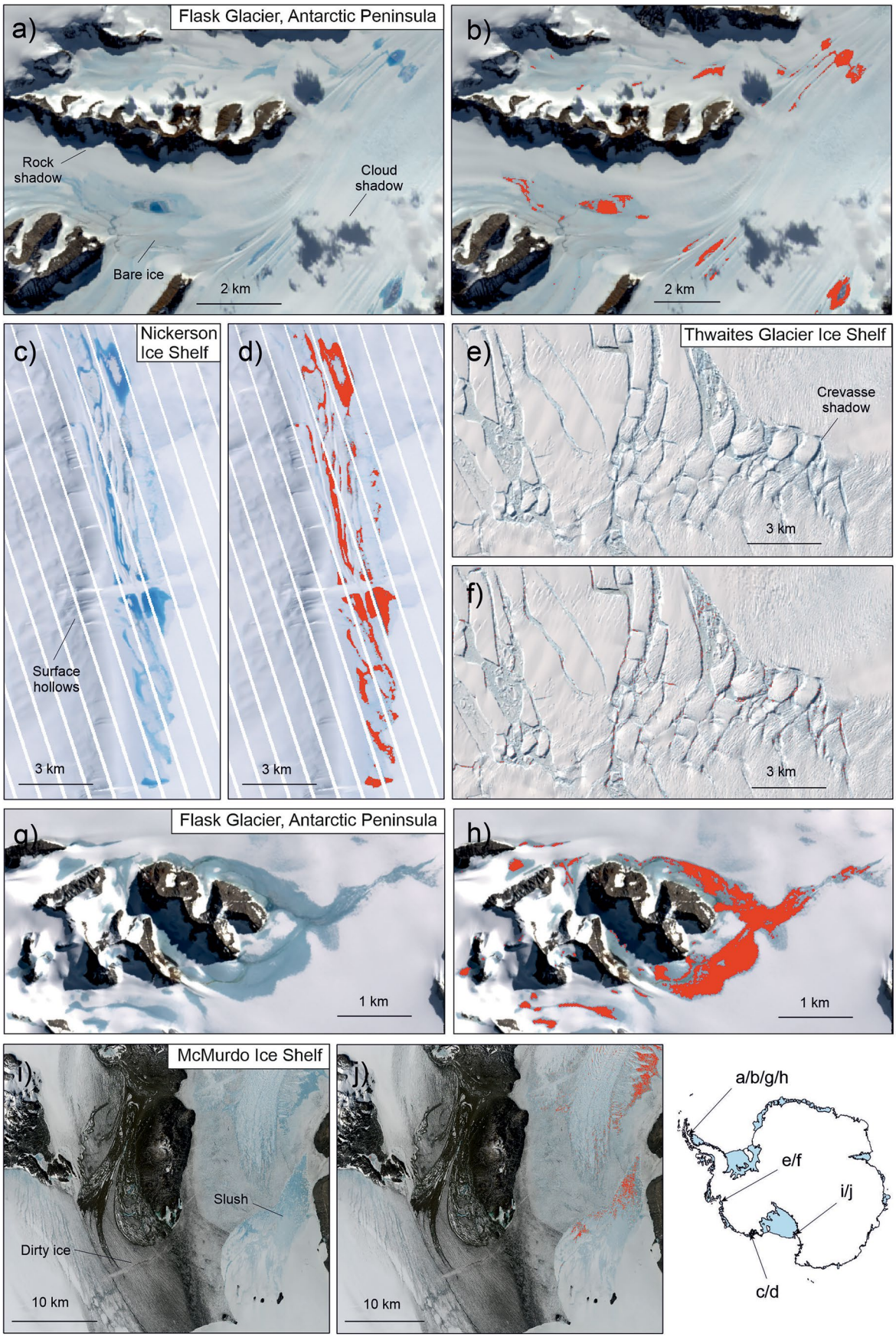

Extended Data Fig. 2 | See next page for caption.

https://doi.org/10.1038/s41558-025-02363-5

Extended Data Fig. 2 | Examples of automated mapping performance for selected images with potentially complex spectral characteristics. (**a, b**) Landsat 8 image of Flask Glacier on the Antarctic Peninsula, 07/02/2016. Note how surface water is successfully differentiated from areas of rock, rock shadow, ice or cloud shadow. (**c, d**) Landsat 7 image of meltwater ponds on Nickerson Ice Shelf, West Antarctica on 04/01/2013. Note how water is identified equally well in Landsat 7, and there are no misclassification errors with shaded surface hollows. (**e, f**) Landsat 8 image of the fracture zone of Thwaites Ice Shelf, 10/01/2019. There are some minor misclassification errors in areas of crevasse shadow, but these are spatially limited and did not have had a notable influence on West Antarctic Ice Sheet area totals (Supplementary Discussion 5). (**g, h**) Landsat 8 image of slush immediately south of Flask Glacier, from 03/03/2016. Note how large areas of slush, in addition to surface lakes, are captured by the threshold-based method. (**i, j**) Landsat 8 image of McMurdo Ice Shelf, 02/01/2017. Note how some surface water features have been missed, but dirty ice has not been mistaken for surface water. Ice-sheet and ice-shelf boundaries from ref. 56. Background satellite imagery from Google Earth Engine under a Creative Commons licence CC BY 4.0.

https://doi.org/10.1038/s41558-025-02363-5

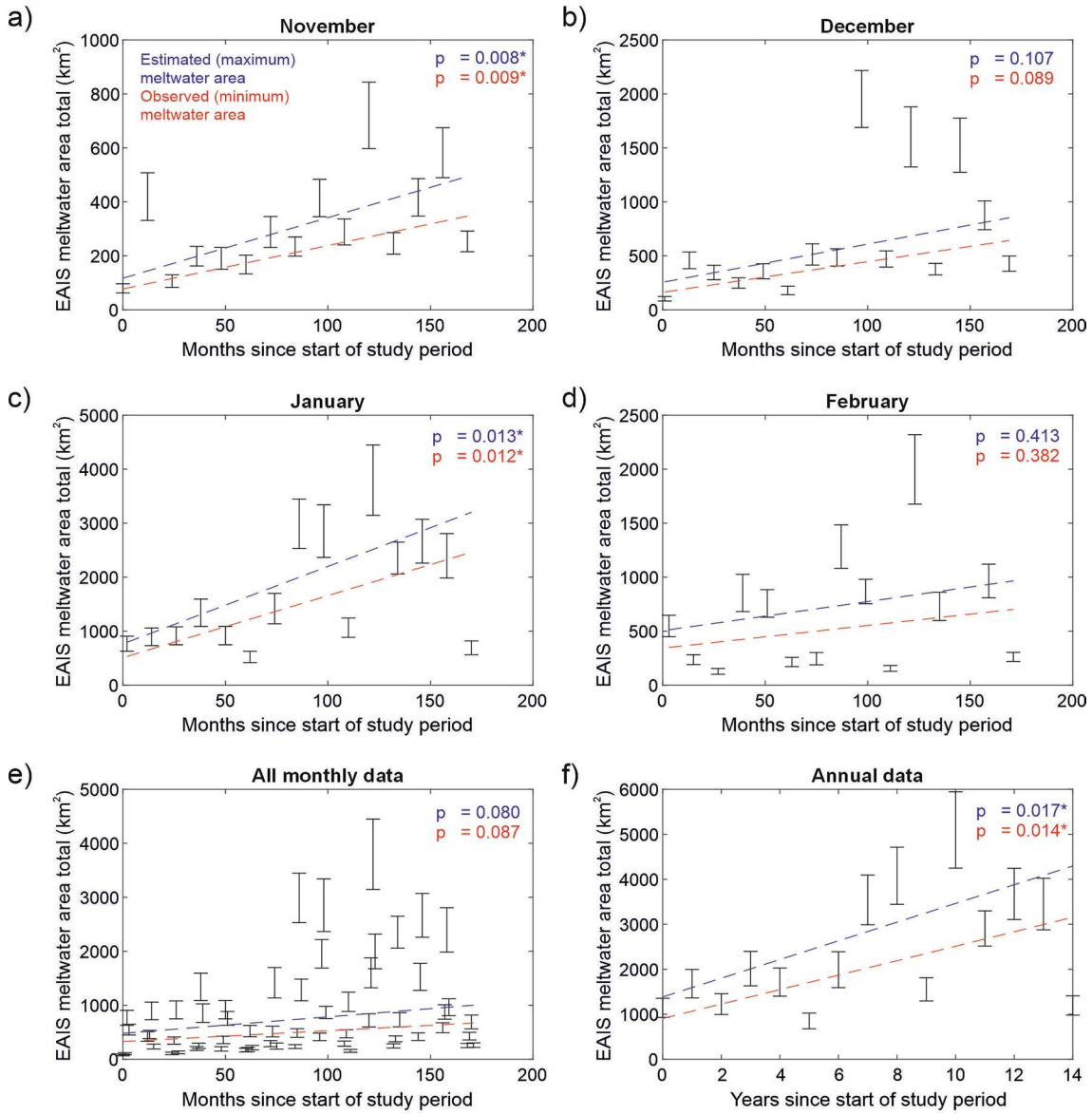

Extended Data Fig. 3 | Robust linear regression of surface meltwater area through time for the East Antarctic Ice Sheet. (**a**–**d**) Regression plots for the individual months of November – February. (**e**) Regression plot showing all the individual monthly data together. (**f**) Regression plot for the overall total areas of meltwater covered each melt season (November – February). For each plot, vertical bars indicate the range between 'observed minimum' and 'estimated maximum' meltwater area values. Regression lines for both observed (red) and estimated (blue) data are displayed, along with significance p-values. Asterisks indicate regressions that are statistically significant to $p < 0.05$.

https://doi.org/10.1038/s41558-025-02363-5

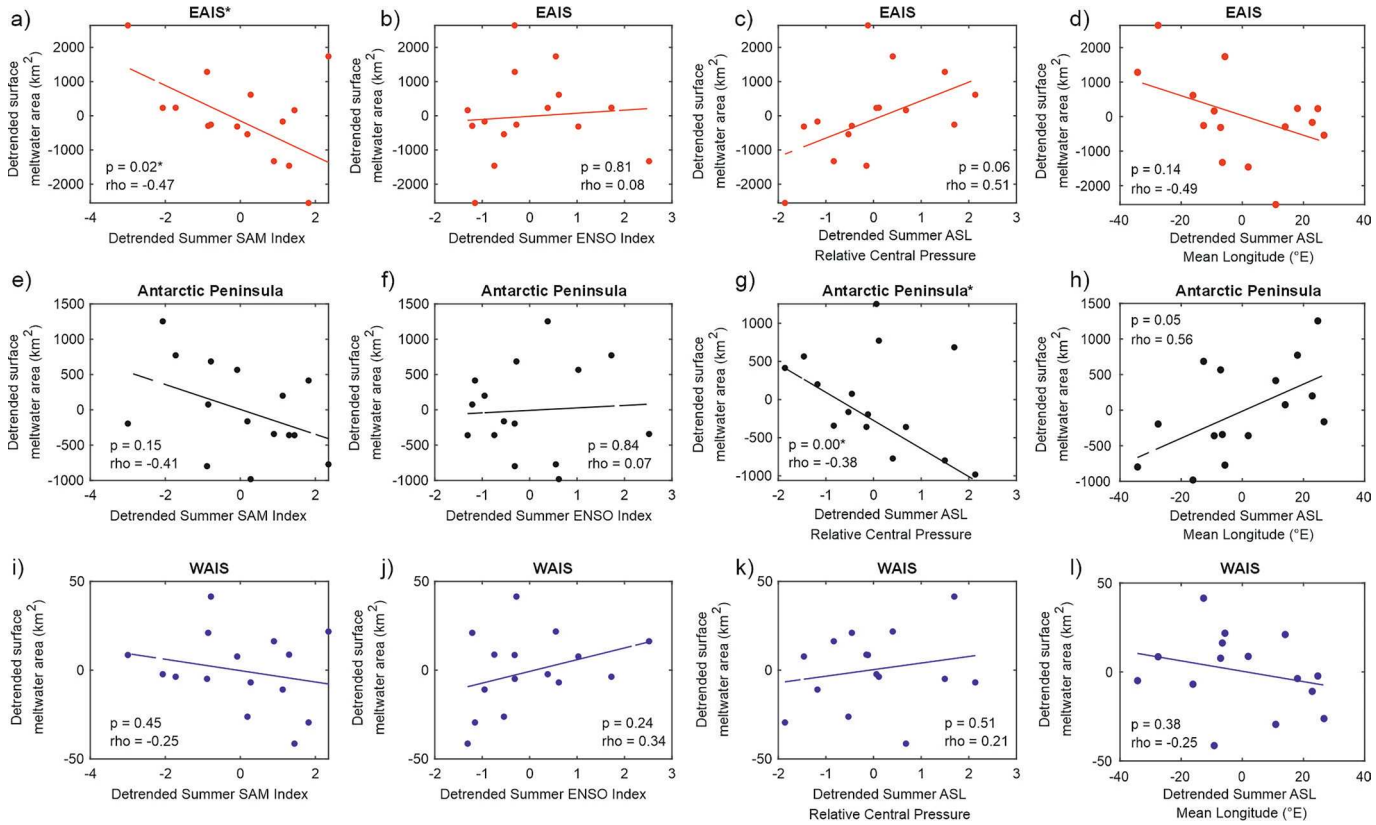

Extended Data Fig. 4 | Scatter plots showing the relationship between annual maximum surface meltwater area and three climate indices. Climate indices: 1) SAM Index (**a, e, i**); 2) Oceanic Nino Index (**b, f, j**); 3) ASL relative central pressure (**c, g, k**) and longitude (**d, h, l**). The three rows display results for the EAIS (red), AP (black) and WAIS (blue) respectively. Surface meltwater area and climate index data were detrended prior to conducting linear regression. Significant relationships ($p < 0.05$) are indicated by an asterisk next to the plot title (**a**,**g**).

https://doi.org/10.1038/s41558-025-02363-5

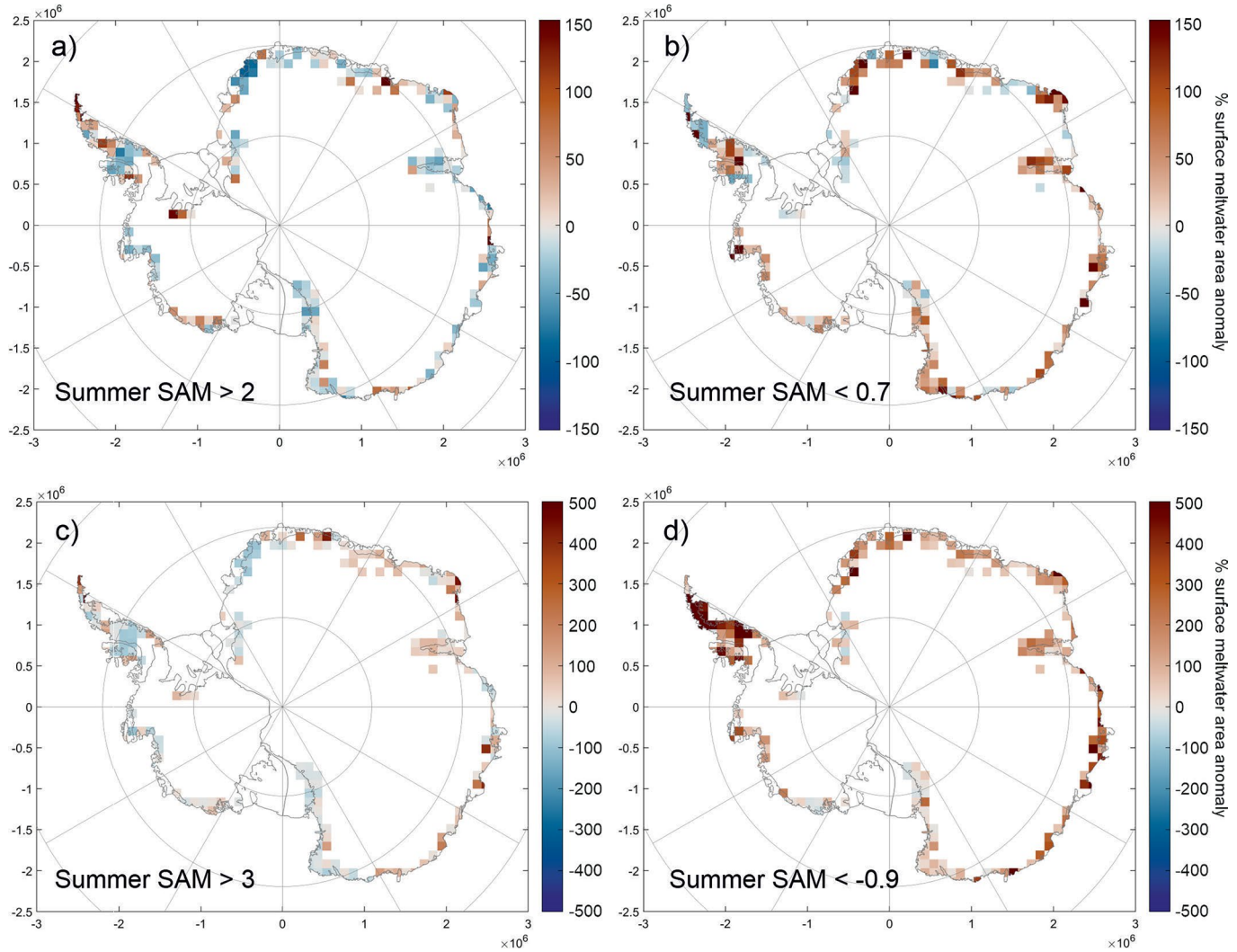

Extended Data Fig. 5 | Composite maps displaying surface meltwater area percentage anomalies across Antarctica, based on selected summer Southern Annuar Mode index thresholds. (**a**) Greater than 2 (n = 6); (**b**) lower than 0.7 (n = 6); (**c**) greater than 3 (n = 2); (**d**) lower than -0.9 (n = 2); see Extended Data Table 2 for index values. For each composite plot, the number of years satisfying the criteria is displayed in brackets. Note the change in scale between plots **a**-**b** and plots **c**-**d**. Anomaly values are relative to the 15-year average. Ice-sheet and ice-shelf boundaries from ref. 56.

https://doi.org/10.1038/s41558-025-02363-5

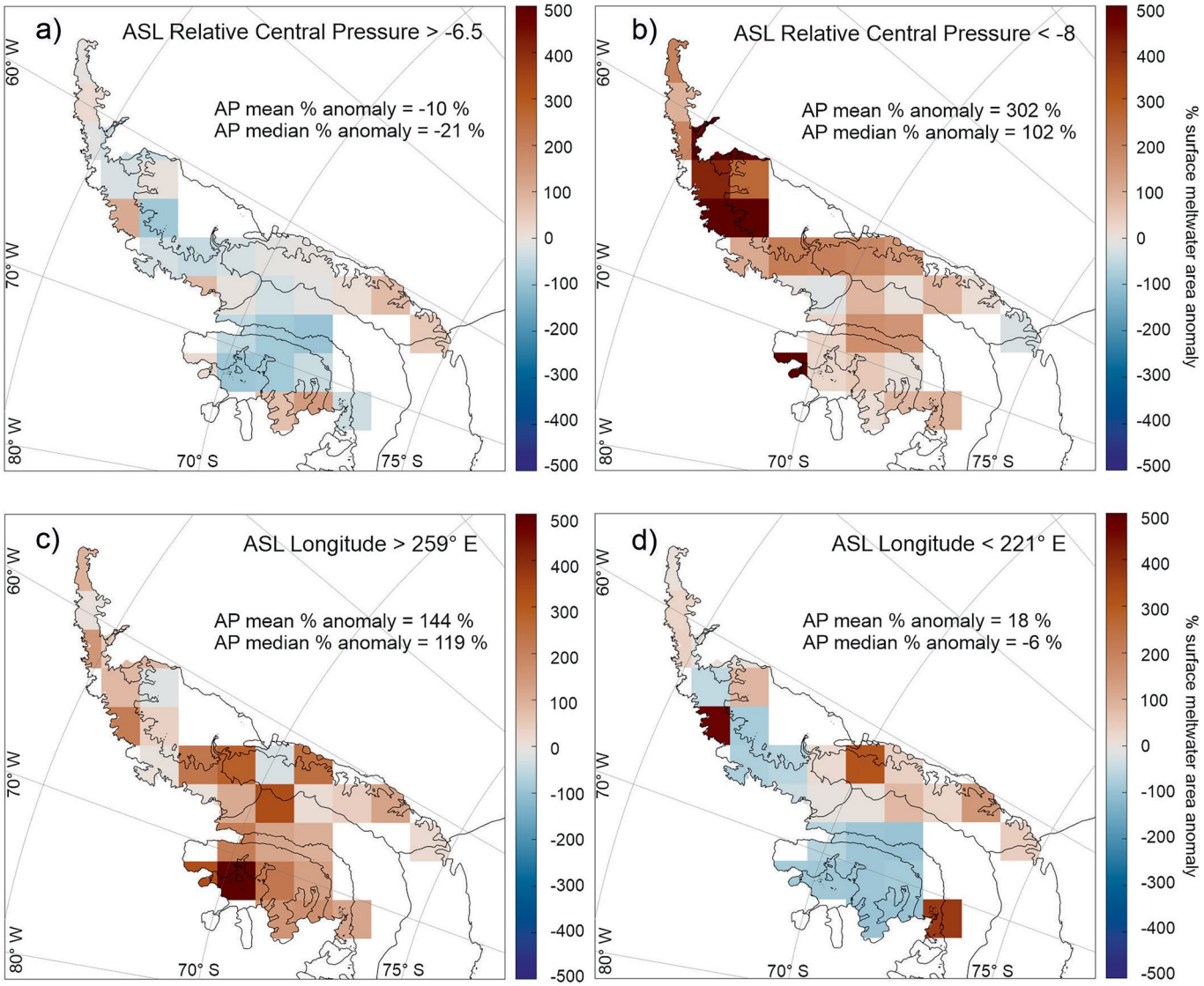

Extended Data Fig. 6 | Composite maps displaying surface meltwater area percentage anomalies on the Antarctic Peninsula for selected Amundsen Sea Low conditions. The top plots display anomaly values for the highest (**a**) and lowest (**b**) three years of ASL relative central pressure throughout the study period. The bottom plots show surface meltwater area anomalies for when the ASL central longitude is closer (**c**) or further away from the Antarctic Peninsula (**d**). Anomaly values are relative to the 15-year average. Ice-sheet and ice-shelf boundaries from ref. 56.

https://doi.org/10.1038/s41558-025-02363-5

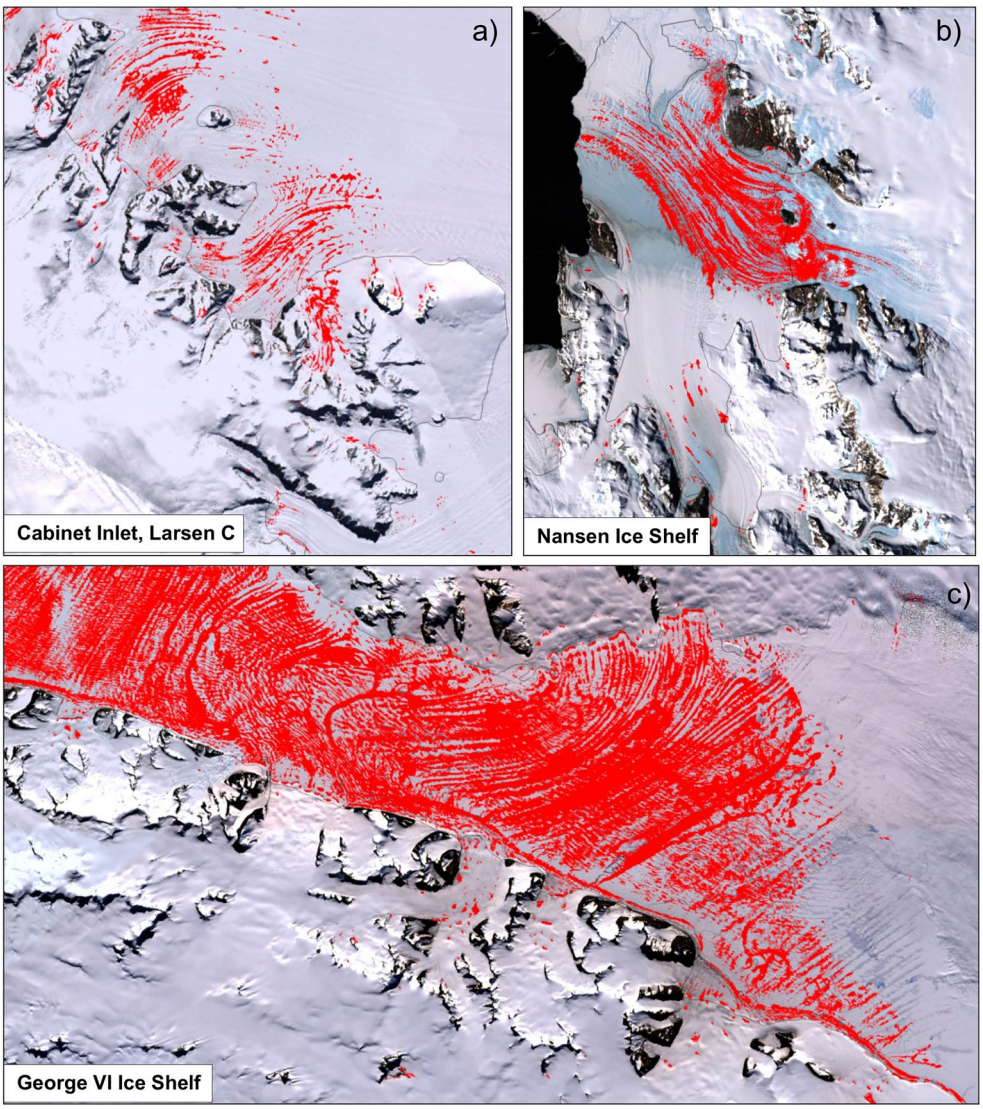

Extended Data Fig. 7 | Examples of maximum surface meltwater extent throughout our study period. Maximum extent composites of surface meltwater (red) between 2006 – 2021 for Cabinet Inlet, Larsen C (**a**), Nansen Ice Shelf (**b**) and George VI Ice Shelf (**c**). The background image in each example is the Landsat Mosaic Image of Antarctica (LIMA). Note how there are no obvious examples of rock, or rock shadow, being misclassifed as surface meltwater. Background satellite imagery from the United States Geological Survey under a Creative Commons licence CC BY 4.0.

https://doi.org/10.1038/s41558-025-02363-5

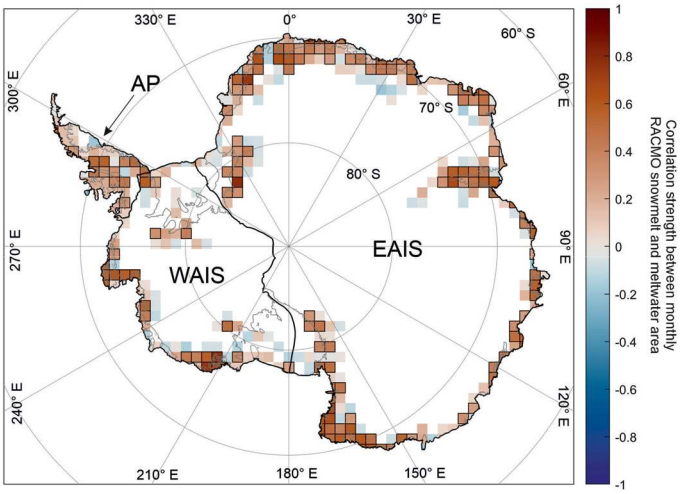

Extended Data Fig. 8 | Correlation strength between monthly modelled melt and surface meltwater area, per 108 km square grid tile. Correlations are displayed for tiles where surface meltwater was mapped on at least five separate months throughout the study period. Tiles with a black outline indicate statistically significant correlations ($p < 0.05$). The thick black line marks the boundaries between the EAIS, WAIS and AP. Ice-sheet and ice-shelf boundaries from ref. 56.